Functional reconstitution of vacuolar H^+-ATPase from V_o proton channel and mutant V_1-ATPase provides insight into the mechanism of reversible disassembly

Received for publication, January 16, 2019, and in revised form, February 10, 2019 Published, Papers in Press, February 21, 2019, DOI 10.1074/jbc.RA119.007577

Stuti Sharma[1], **Rebecca A. Oot, Md Murad Khan, and Stephan Wilkens**[2]

From the Department of Biochemistry & Molecular Biology, SUNY Upstate Medical University, Syracuse, New York 13210

Edited by Karen G. Fleming

The vacuolar H^+-ATPase (V-ATPase; V_1V_o-ATPase) is an ATP-dependent proton pump that acidifies subcellular compartments in all eukaryotic organisms. V-ATPase activity is regulated by reversible disassembly into autoinhibited V_1-ATPase and V_o proton channel subcomplexes, a process that is poorly understood on the molecular level. V-ATPase is a rotary motor, and recent structural analyses have revealed different rotary states for disassembled V_1 and V_o, a mismatch that is likely responsible for their inability to reconstitute into holo V-ATPase *in vitro*. Here, using the model organism *Saccharomyces cerevisiae*, we show that a key impediment for binding of V_1 to V_o is the conformation of the inhibitory C-terminal domain of subunit H (H_{CT}). Using biolayer interferometry and biochemical analyses of purified mutant V_1-ATPase and V_o proton channel reconstituted into vacuolar lipid-containing nanodiscs, we further demonstrate that disruption of H_{CT}'s V_1-binding site facilitates assembly of a functionally coupled and stable V_1V_o-ATPase. Unlike WT, this mutant enzyme was resistant to MgATP hydrolysis-induced dissociation, further highlighting H_{CT}'s role in the mechanism of V-ATPase regulation. Our findings provide key insight into the molecular events underlying regulation of V-ATPase activity by reversible disassembly.

The vacuolar H^+-ATPase (V-ATPase, V_1V_o-ATPase)[3] is an ATP-dependent proton pump found on the endomembrane system of all eukaryotic organisms. This multisubunit nanomotor acidifies subcellular compartments and, in certain specialized tissues, the extracellular space. V-ATPase is essential for vital cellular processes such as pH homeostasis, protein sorting, autophagy, endocytosis, mTOR, and Notch signaling, as well as bone remodeling, urine acidification, hormone secretion, and neurotransmitter release (1). Although complete loss of V-ATPase function is embryonic lethal in mammals, aberrant activity has been associated with widespread human diseases including renal tubular acidosis (2), osteoporosis (3), neurodegeneration (4), diabetes (5), male infertility (6), and cancer (7), making V-ATPase a potential drug target (8, 9). However, because of its essential nature, global inhibition of V-ATPase is not a therapeutic option. Instead, there is a need for targeted modulation of the enzyme's activity, a goal that requires a detailed understanding of V-ATPase's catalytic and regulatory mechanisms.

V-ATPase is composed of two subcomplexes, a cytosolic ATPase called V_1, and a membrane integral proton channel termed V_o (Fig. 1*A*). In yeast, the subunit compositions for the V_1 and V_o are $A_3B_3(C)DE_3FG_3H$ and $ac_8c'c''def$, respectively (10). The A and B subunits of V_1 are arranged in a hexamer (A_3B_3), with three catalytic sites at alternating AB interfaces. Located within the hexamer and extending from it in the direction of the membrane is subunit D that, together with F, provides the functional link between V_1 and V_o. The V_o is constituted by subunit *a* that can be divided into cytosolic N-terminal and membrane-integral C-terminal domains (a_{NT} and a_{CT}), the *c*, *c*′ and *c*″ subunits ("proteolipids") that form a ring (*c*-ring), and subunit *d* that connects the *c*-ring with V_1 subunits D and F. V_1 and V_o are held together by three heterodimers of subunits E and G (peripheral stalks EG1–3) that link the catalytic hexamer and the single copy C and H subunits to the membrane integral *a* subunit by binding to a_{NT}.

V-ATPase is a rotary motor enzyme and employs a catalytic mechanism that is shared with the F-, A-, and A/V-type ATPases (11). In V-ATPase, ATP hydrolysis– driven rotation of the DF*dc*-ring central rotor is coupled to proton translocation at the interface of a_{CT} and the *c*-ring. During catalysis, the three peripheral stalks, in conjunction with C, H, and a_{NT}, resist the rotary torque to keep the A_3B_3 hexamer static against a_{CT} for efficient energy coupling. However, unlike F-, A-, and A/V-type enzymes, eukaryotic V-ATPase is regulated by a unique mechanism referred to as "reversible disassembly," wherein V_1 detaches from V_o in response to *e.g.* nutrient shortage (12–14) (Fig. 1*B*), with concomitant silencing of V_1's MgATPase (15, 16), and V_o's proton transport activities (17, 18). First described in yeast and insect, reversible disassembly is now emerging as an important and conserved regulatory mechanism, having

This work was supported by National Institutes of Health Grant GM058600 (to S. W.). The authors declare that they have no conflicts of interest with the contents of this article. The content is solely the responsibility of the authors and does not necessarily represent the official views of the National Institutes of Health.

This article contains Figs. S1–S5.

[1] Present address: Dept. of Cell Biology, Harvard Medical School, 250 Longwood Ave., Boston, MA 02115.

[2] To whom correspondence should be addressed: Dept. of Biochemistry & Molecular Biology, SUNY Upstate Medical University, Syracuse, NY 13210. Tel.: 215-464-8703; Fax: 315-464-8750; E-mail: wilkenss@upstate.edu.

[3] The abbreviations used are: V-ATPase, vacuolar H^+-ATPase; V_1, ATPase sector of the V-ATPase; V_o, membrane sector of the V-ATPase; a_{NT}, N-terminal cytoplasmic domain of the *a* subunit; a_{CT}, C-terminal transmembrane domain of the *a* subunit; H_{CT}, C-terminal domain of the H subunit; H_{NT}, N-terminal domain of the H subunit; MBP, maltose-binding protein; BLI, biolayer interferometry; ConA, concanamycin A; MSP, membrane scaffold protein.

© 2019 Sharma et al. Published under exclusive license by The American Society for Biochemistry and Molecular Biology, Inc.

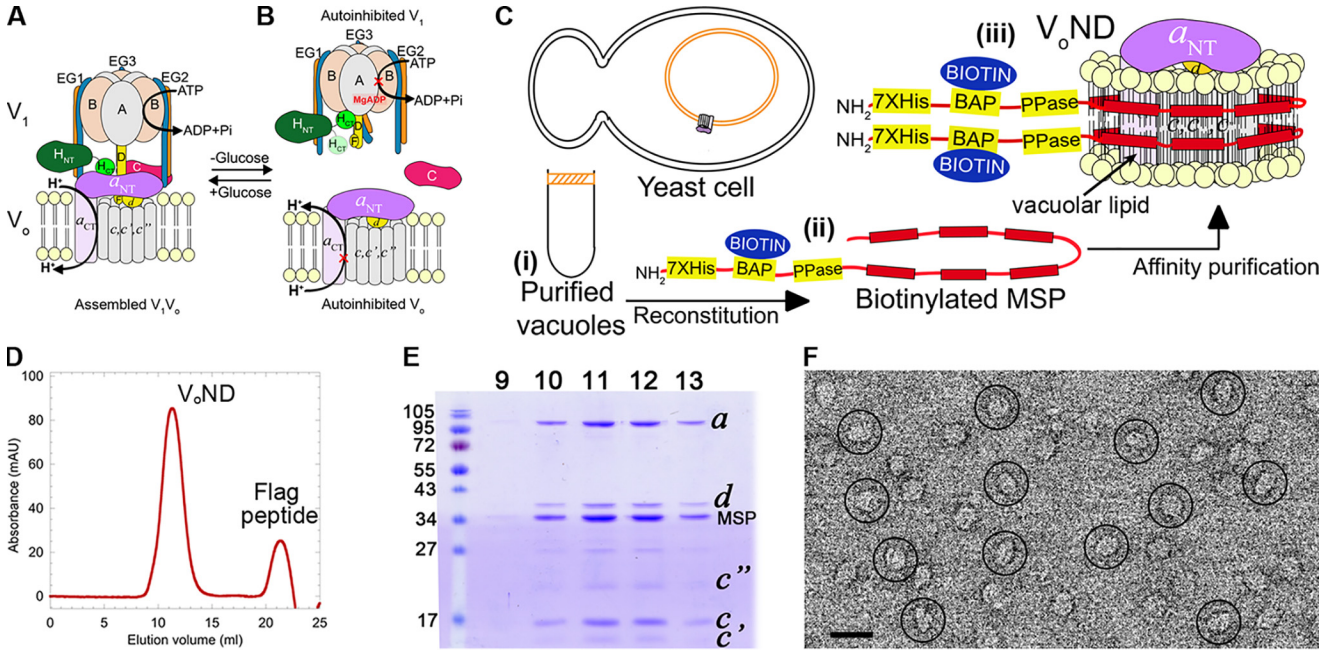

Figure 1. Purification and characterization of V_oND. *A* and *B*, schematic of V-ATPase regulation by reversible disassembly. *C*, purification strategy. Yeast vacuoles are isolated by flotation on a Ficoll gradient (*panel i*). Detergent-solubilized vacuolar proteins are mixed with biotinylated MSP (*panel ii*) and reconstituted into lipid nanodiscs followed by α-FLAG affinity capture of V_oND (*panel iii*). *D*, size-exclusion chromatography of V_oND. *E*, peak fractions were resolved using SDS-PAGE. *F*, negative stain EM of purified V_oND. *Bar*, 20 nm.

been observed in mammalian systems as well (19–21). However, although we have some understanding of the process at the cellular level (22), less is known about the mechanism of reversible disassembly at the molecular scale. Biochemical studies in yeast have shown that the single copy C and H subunits, which are unique to eukaryotic V-ATPase, play key roles in enzyme regulation. Both C and H are two-domain proteins, with C composed of "foot" (C_{foot}) and "head" (C_{head}), and H of N- (H_{NT}) and C-terminal (H_{CT}) domains. H has a dual role because it is required for both coupling MgATPase to proton-pumping activities and for stabilizing the autoinhibited state of membrane detached V_1; C functions to stabilize the V_1–V_o interface in the holo enzyme but dissociates from the complex upon regulated disassembly. Recent structural studies have revealed that in assembled V_1V_o, H_{CT} is bound to a_{NT} (23), an interaction required for energy coupling (24) (Fig. 1*A*). Upon disassembly of V_1 from V_o, H_{CT} undergoes a 150° rotation to wedge an inhibitory loop between the B subunit of an open catalytic site and subunits DF of the central rotor (16) (Fig. S1, *A–D, red spheres*). At the same time, a_{NT} moves from its peripheral position near C_{foot} and EG in V_1V_o (Fig. 1*A*) toward a more central position in free V_o to bind subunit *d* (18, 25–27) (Fig. S1, *E–G*). Moreover, cryoEM models of three distinct rotary states of holo V-ATPase (states 1–3) (23), along with the structures of autoinhibited V_1 (16) and V_o (25, 27), revealed that although V_1 is halted in state 2, V_o adopted state 3 (10) (Fig. S1). We hypothesized that the mismatch of rotational states observed in autoinhibited V_1 and V_o, together with the large conformational changes of H_{CT} and a_{NT} that accompany enzyme dissociation, explain why V_1 does not readily rebind free V_o under physiological conditions *in vitro* (10, 28), a safety mechanism that likely evolved to prevent spontaneous reassembly *in vivo* when the disassembled, inactive state is required.

We recently introduced biolayer interferometry (BLI) of purified V-ATPase in biotinylated and native lipid containing nanodiscs to analyze MgATP-dependent enzyme dissociation kinetics (29). Here, we have expanded on this approach to probe the interaction of V_1 and V_o. V_o sector was reconstituted into vacuolar lipid containing nanodiscs (V_oND) and immobilized on BLI sensors to screen V_1 mutants for their ability to bind V_o. In line with available literature (28), WT V_1 did not bind to V_oND, presumably because of the "state mismatch" observed in the structures of free V_1 and V_o (10). Previously, we generated a chimeric H subunit containing the yeast N-terminal and human C-terminal domains (H_{chim}) that does not inhibit free V_1 because human H_{CT} lacks an inhibitory loop that links an open catalytic site and the central rotor (16), and consequently, V_1 containing H_{chim} is not restrained in any particular rotational state. We show that replacement of endogenous H in yeast V_1 with H_{chim} (V_1H_{chim}) (16) permits binding to V_oND, and formation of a coupled holo V-ATPase ($V_1H_{chim}V_oND$) with catalytic properties similar to the ones of the recently characterized WT V_1V_oND (29). However, $V_1H_{chim}V_oND$ was more resistant to ATP hydrolysis-induced disassembly compared with WT, highlighting the importance of H_{CT}'s conformational switch in driving V-ATPase disassembly. The *in vitro* data presented here thus provide key insight into the molecular steps that accompany V-ATPase regulation by reversible disassembly.

Results

Purification and characterization of native lipid nanodisc reconstituted V_o (V_oND) and V_1 mutants

V_o was extracted from yeast vacuoles using the "reconstitution before purification" strategy as described for V_1V_o (29) (Fig. 1*C*, *panels i–iii*). The resultant V_oND complex consisted of V_o embed-

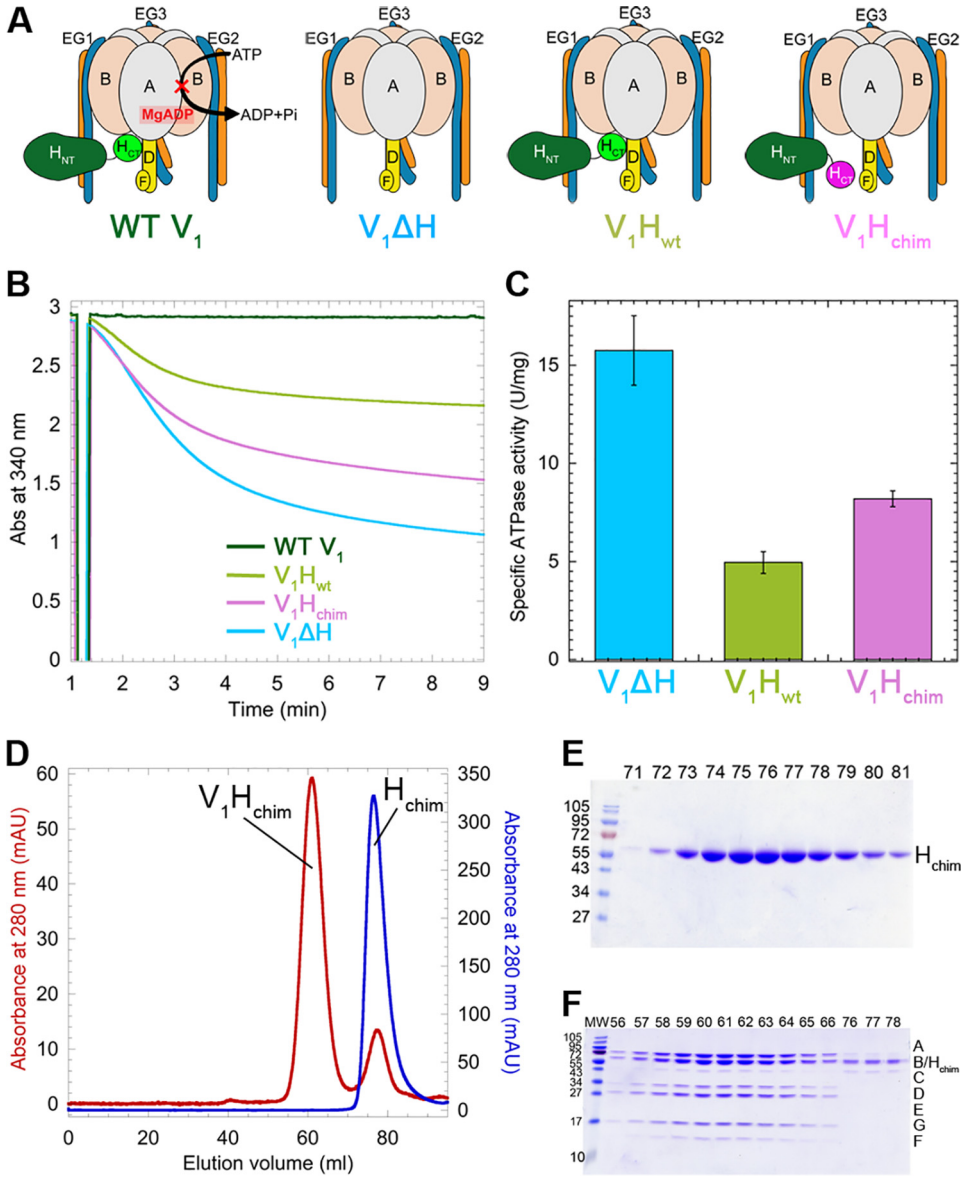

Figure 2. Purification and characterization of V_1 mutants. *A*, schematic representation of the V_1 mutants. *B*, time-dependent MgATPase activities of the V_1 mutants measured in an ATP regenerating assay. *C*, specific activities of the V_1 mutants ± S.E. from at least two independent purifications per mutant. *D*, size-exclusion chromatography of H_{chim} (*blue trace*) and $V_1\Delta H$ reconstituted with H_{chim} (V_1H_{chim}, *red trace*). *E* and *F*, SDS-PAGE of column fractions of H_{chim} (*E*) and V_1H_{chim} (*F*).

ded in endogenous vacuolar lipid containing nanodiscs encircled by biotinylated membrane scaffold protein (MSP; Fig. 1*C*, *panel iii*). The purified complex was monodisperse and contained all V_o subunits plus MSP based on gel filtration and SDS-PAGE (Fig. 1, *D* and *E*). Examination of purified V_oND using negative stain EM showed single particles of V_oND with the typical size and appearance as described previously (26) (Fig. 1*F*).

Four different V_1 mutants were tested for their ability to bind V_oND and form coupled holo V-ATPase (Fig. 2*A*): WT V_1 (containing subunits $A_3B_3DE_3FG_3H$), V_1 purified from a yeast strain deleted for subunit H ($V_1\Delta H$), $V_1\Delta H$ reconstituted with recombinantly expressed WT H (V_1H_{wt}), and $V_1\Delta H$ reconstituted with chimeric H (V_1H_{chim}) (16). Although WT V_1 has no measurable MgATPase activity (Fig. 2*B*, *dark green trace*), $V_1\Delta H$ had an initial specific activity of 15.7 ± 1.7 units/mg, consistent with previous reports (16, 30) (Fig. 2, *B* and *C*, *blue trace* and *bar*). Although MgATPase activity is measured in an ATP-regenerating system, the activity of $V_1\Delta H$ decreases over time as MgADP gets trapped in a closed catalytic site, leading to the MgADP-inhibited state (15). Although V_1H_{wt} has identical subunit composition to WT V_1, V_1H_{wt} distinguishes itself from WT by having only ~0.4 instead of 1.3 mol/mol ADP in catalytic sites (16), and the complex therefore exhibits an initial MgATPase activity of ~4.95 ± 0.55 units/mg before becoming MgADP-inhibited (Fig. 2, *B* and *C*, *light green*). $V_1\Delta H$ reconstituted with H_{chim} to yield V_1H_{chim} (Fig. 2, *D–F*) showed an initial MgATPase activity of 8.2 ± 0.4 units/mg that, as for the other V_1 mutants, declined over time because of MgADP inhibition (Fig. 2, *B* and *C*, *pink*).

Binding of C subunit to V_1

Experiments in yeast have shown that upon deletion of the gene encoding the C subunit, V_1 does not stably/functionally

associate with V_o. Moreover, biochemical analysis revealed that C_{head} binds isolated EG heterodimer with moderate affinity, whereas both C_{foot} and EG bind a_{NT} weakly (31, 32). From these data we concluded that V_1 and V_o are held together by multiple weak interactions, resulting in an overall high-avidity interface, and that destabilization of one of these interactions by a cellular response to starvation would result in enzyme dissociation (10, 32). More recently we showed that although H_{NT} binds isolated EG with a K_d of ~0.2 μM, the affinity of the interaction is increased 40-fold when EG is part of V_1 (30). Moreover, when we analyzed binding of H (and H_{NT}) to $V_1\Delta H$, we found that MgATP hydrolysis destabilized the V_1–H interaction, an effect likely caused by the cyclic conformational changes at the catalytic AB interfaces to which the EG heterodimers are bound (30). We therefore wished to determine whether C binding to EG on V_1 is also enhanced compared with isolated EG, and if so, (i) what the affinity of the interaction is, and (ii) whether the interaction is also destabilized during ATP hydrolysis. Because V_1 isolated from starving yeast has varying levels of substoichiometric amounts of C bound (15, 16, 33, 34), we purified V_1 from a yeast strain in which C was deleted ($V_1\Delta C$) (16) to test for C binding. Using a BLI setup similar to the one we recently employed to analyze binding of H (and H_{NT}) to $V_1\Delta H$ (30), we found that $V_1\Delta C$ binds C with a K_d of ~0.7 nM (Fig. S4), indicating that one of the EG heterodimers bound to V_1 is in a conformation that is more favorable for C binding compared with the isolated heterodimer. However, to test whether C binding is also destabilized as a result of ATP hydrolysis, we could not use $V_1\Delta C$ because it contains the H subunit and so has no MgATPase activity, and we therefore used the catalytically active V_1H_{chim} instead. As seen for the V_1–H interaction, dissociation of V_1H_{chim} from MBP-C loaded sensors was greatly accelerated only when the sensors were dipped into wells containing MgATP. Fitting the subunit C release in MgATP to two exponentials revealed a fast off rate of ~$0.012 \pm 2.3 \times 10^{-5}$ s^{-1} and a slower off rate of $5.1 \times 10^{-4} \pm 2 \times 10^{-6}$ s^{-1}, values similar to those observed for MgATP hydrolysis induced subunit H release as reported earlier (30) (Fig. S5). This suggests that the *in vivo* dissociation of the C subunit from the vacuolar membrane that occurs as a result of starvation is a direct result of MgATP hydrolysis–induced conformational changes of the EG heterodimer that is bound to C_{head} in the assembled enzyme (EG3) (23, 35). In summary, as for subunit H, binding of C to EG is significantly enhanced when EG is part of V_1, and the V_1–C interaction is greatly destabilized upon ATP hydrolysis.

V_1H_{chim} and C subunit associate with V_oND to form coupled V-ATPase in vitro

The ability of the V_1 mutants depicted in Fig. 2*A* to interact with V_o was tested using BLI. V_oND reconstituted with biotinylated MSP was immobilized on streptavidin-coated BLI sensors (Fig. 3*A*, *step 1*), which were then dipped in wells containing V_1 mutants and subunit C (Fig. 3*A*, *step 2*). We found that of the four V_1 mutants, only V_1H_{chim} showed significant association with V_oND (Fig. 3*A*, *red trace*). The sensors were then dipped in buffer to measure dissociation rates (Fig. 3*A*, *step 3*). However, no significant dissociation was observed, indicating stable assembly of V_1H_{chim} with V_o. Without C, none of the V_1 mutants showed significant binding (Fig. S3), consistent with studies in yeast that showed that deletion of C prevents assembly of V_1V_o (36). As a control, the sensors were then dipped in PreScission protease to cleave and release any remaining complex (Fig. 3*A*, *step 4*). Further, we conducted BLI experiments in which V_oND-coated sensors were first dipped into wells containing a mAb (10D7) against a_{NT}, which recognizes a cryptic epitope only available for binding in free V_o (12), before dipping the sensors into V_1H_{chim} plus C containing wells. Under these conditions, the observed on-rate (k_{obs}) of V_1H_{chim} was significantly (~60-fold) reduced, indicating that the observed BLI signal upon dipping the sensors into V_1H_{chim} plus C was indeed due to binding of V_1H_{chim} to immobilized V_oND (Fig. S2).

Whereas the BLI experiment showed slow, but stable, association of V_1H_{chim} and C with V_oND, it was not clear whether functional V-ATPase was formed under these conditions. To address this question, we monitored MgATPase activity of a 1:1:2 mixture of V_1H_{chim}, V_oND, and C that is sensitive to the V-ATPase specific inhibitor, concanamycin A (ConA), as a function of time (Fig. 3*B*). Although V_1H_{chim} has MgATPase activity on its own, ConA binds to the V_o complex and prevents *c*-ring rotation, so ATPase activity that is abolished by treatment with ConA is evidence of a functionally coupled V-ATPase complex. The experiment demonstrated that binding of V_1H_{chim} and C to V_oND resulted in the formation of a coupled $V_1H_{chim}V_o$ND complex and that the reconstitution under these conditions was complete in ~2 h, with a final specific activity of 7.2 ± 1.09 units/mg, similar to what is reported for purified WT V_1V_oND (6.9 ± 0.6 units/mg) (29) (Fig. 3*B*, *inset*, *pink* and *blue bars*, respectively). The ability of V_1H_{chim} to form a functional complex with V_oND is consistent with the previous observation that H_{chim} can complement deletion of the native H subunit in yeast cells (16). ConA-sensitive ATPase activity was also measured with V_oND, C, and V_1H_{wt} and produced only 0.26 ± 0.2 units/mg of coupled activity (Fig. 3*B*, *inset*, *orange bar*). Therefore, reconstitution of V_1H_{wt} with V_o and C is highly inefficient under these conditions, consistent with earlier *in vitro* studies (28) and the real-time BLI experiments presented here (Fig. 3*A*).

$V_1H_{chim}V_o$ND is more stable in presence of MgATP compared with V_1V_oND

Using BLI, we have previously demonstrated that V_1's dissociation from V_o is negligible under non-ATP hydrolyzing conditions but that in presence of MgATP, the complex undergoes spontaneous dissociation with an off-rate of $1 \times 10^{-3} \pm 3.3 \times 10^{-6}$ s^{-1} (29). We conducted a similar experiment using $V_1H_{chim}V_o$ND, wherein after association of V_1H_{chim} and C with V_oND on BLI sensors, we dipped the sensors in wells containing buffer or 1 mM MgATP. Significantly, unlike WT V_1V_oND, $V_1H_{chim}V_o$ND showed very little to no dissociation in the presence of MgATP, indicating that the assembled $V_1H_{chim}V_o$ND complex is inherently more stable than the WT complex (Fig. 3*C*). The experiment thus highlights the importance of H_{CT}'s conformational switch (from energy coupling in the holo enzyme to autoinhibition of membrane detached V_1) in driving V-ATPase disassembly.

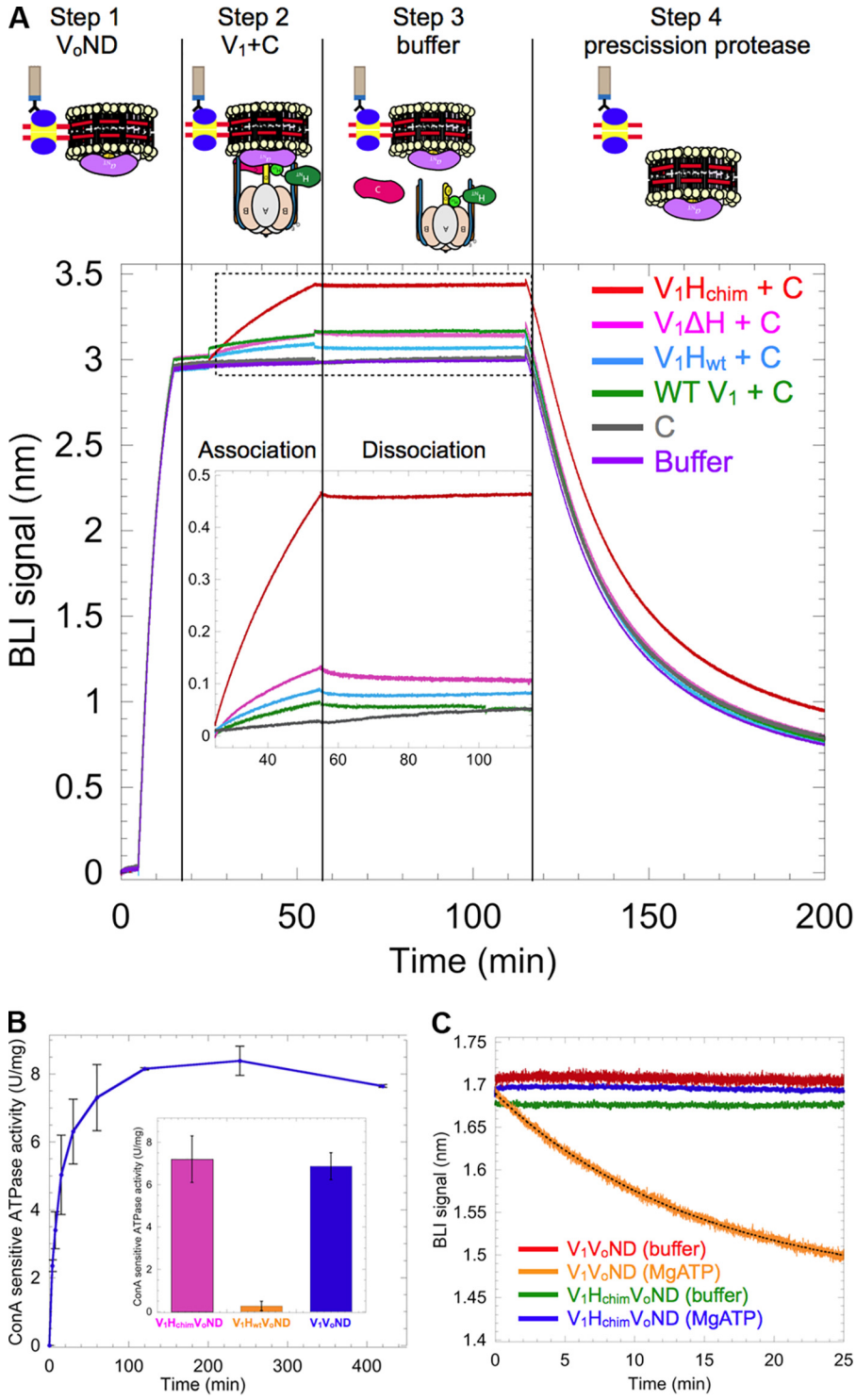

Figure 3. V_1H_{chim} and C associate with V_oND to form coupled V_1V_o-ATPase. *A*, V_oND was immobilized on streptavidin-coated BLI sensors via biotinylated MSP (*step 1*). Sensors were then dipped into 0.4 μM of V_1 mutants in presence of 1 μM C (association; *step 2*) followed by buffer (dissociation; *step 3*). Association with V_oND was most efficient with V_1H_{chim} (*red trace*). Sensors were then dipped in PreScission protease to verify that the BLI signal was not due to nonspecific binding (*step 4*). *Inset* shows an enlarged view of the association and dissociation steps. *B*, equimolar amounts of V_1H_{chim} and V_oND, and a 2-fold molar excess of C subunit were incubated at 22 °C, and the ConA-sensitive MgATPase activity was measured as a function of time. Each point represents the mean ± S.E. of two separate reconstitutions from two individual purifications. *Inset*, specific MgATPase activities of reconstituted $V_1H_{chim}V_oND$ and $V_1H_{wt}V_oND$ (± S.E. from two independent purifications) compared with purified V_1V_oND (29). *C*, following association of the $V_1H_{chim}V_oND$ complex, sensors were dipped in wells containing buffer (*green*) or buffer + 1 mM MgATP (*blue*) for dissociation rate measurement. The dissociation phase of WT V_1V_oND in buffer (*red*) and buffer +1 mM MgATP (*orange*) is included for comparison (data from Ref. 29).

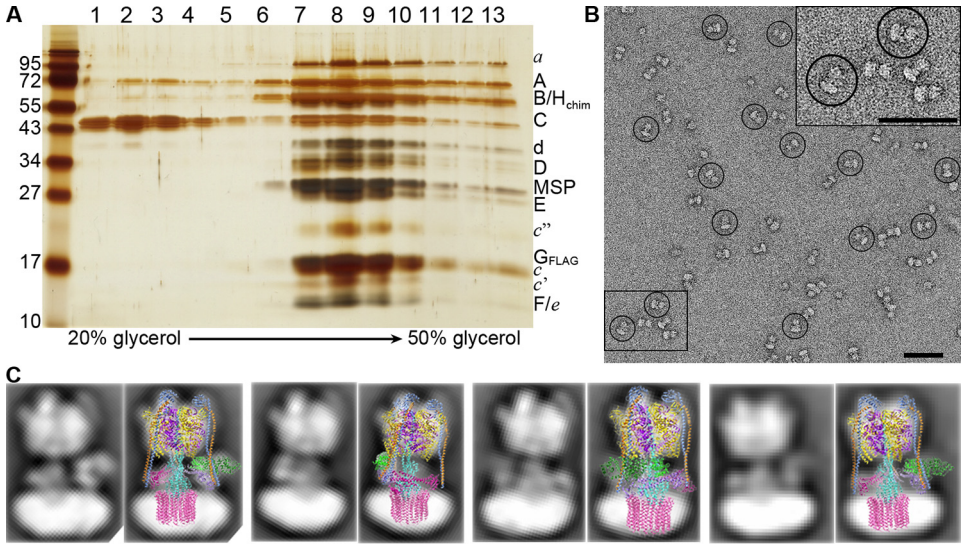

Figure 4. Structural and functional characterization of the $V_1H_{chim}V_oND$ complex. *A*, reconstituted $V_1H_{chim}V_oND$ was subjected to glycerol gradient centrifugation, and the gradient fractions were analyzed by silver-stained SDS-PAGE. *B*, negative stain EM of $V_1H_{chim}V_oND$ showing homogeneous and monodisperse dumbbell-shaped molecules. *Inset* in the *top right* shows 2× zoomed area highlighted in the *bottom left*. *C*, a data set of ~5800 particle projections was subjected to reference-free alignment and classification, and selected class averages were overlaid with projections of the cryoEM model of yeast V_1V_o (Protein Data Bank code 3J9U). *Bars* in *B*, 50 nm.

Structural and functional characterization of $V_1H_{chim}V_oND$

To determine the efficiency of $V_1H_{chim}V_oND$ complex formation, equimolar amounts of V_1H_{chim} and V_oND with a 2-fold molar excess of C were incubated for up to 16 h at 22 °C, and the reconstitution mixture was resolved by glycerol density gradient centrifugation. SDS-PAGE of the gradient fractions showed that the majority of V_1 and V_o subunits co-migrated to fractions 7–10, similar to what was observed for purified WT V_1V_oND (29), with the excess C subunit remaining in lighter fractions (Fig. 4*A*). Negative stain EM of the peak fractions showed single particles of $V_1H_{chim}V_oND$, with the typical dumbbell-shaped appearance of holo V-ATPase reported previously (29, 37, 38) (Fig. 4*B*). A more detailed analysis indicated a good match between averages obtained by reference free alignment and classification of a small data set of $V_1H_{chim}V_oND$ and corresponding projections of a cryoEM map of yeast V_1V_o (23) (Fig. 4*C*). Taken together, these data show that reconstitution of V_1H_{chim} with V_oND and C result in a stable and coupled holo V-ATPase that is structurally similar to the WT enzyme.

Discussion

In our experiments, only V_1H_{chim} (in presence of C) shows significant binding to V_o. As mentioned earlier, human H_{CT} lacks the inhibitory loop found in yeast H_{CT} (16) (Fig. S1, *A–D, red spheres*), consistent with H_{chim}'s inability to inhibit $V_1\Delta H$'s MgATPase activity (Fig. 2, *B* and *C*). This lack of inhibition by H_{chim} is likely due to reduced binding of human H_{CT} to the open catalytic site at the bottom of the A_3B_3 hexamer, with the remaining binding interaction between H_{chim} and V_1 being mediated by H_{NT}'s interaction with one of the EG peripheral stalks. Therefore, we conclude that for V_1 to reconstitute with V_o, H_{CT} must be released from its inhibitory position on V_1, so that H_{CT} is available for binding to V_o's a_{NT}. It is known that upon disassembly of V_1 from V_o, a_{NT} moves from a peripheral position in V_1V_o to a more central position in autoinhibited V_o, where it binds subunit *d* (18, 25–27) (Fig. S1, *E–G*). The observation that V_1H_{chim}, C, and autoinhibited V_oND are sufficient to form a structurally and functionally coupled V-ATPase suggests that the release of H_{CT} from its autoinhibitory position on V_1 is necessary and sufficient for efficient reassembly of V_1 and V_o. Our finding is consistent with the fact that reassembly of V_1 with V_o on vacuoles is not inhibited by ConA, an inhibitor of *c*-ring rotation in the V_o sector (14).

H_{NT} and H_{CT} occupy specific binding sites on free V_1, with H_{NT} bound to EG1 and H_{CT} bound to the bottom of the A_3B_3 hexamer, with its inhibitory loop wedged between the B subunit of an open catalytic site and the central stalk (Fig. S1, *A–D*) (16). The specific interaction of H_{CT} with an open catalytic site maintains inhibitory MgADP in the adjacent closed catalytic site, locking autoinhibited V_1 in rotational state 2. We have recently observed that transient MgATP hydrolysis on V_1H_{wt}, which, unlike WT V_1, is not in the MgADP-inhibited state (Fig. 2*B*), lowers H's affinity for V_1, and we reasoned that this destabilization of the V_1–H interaction is caused by MgATP hydrolysis driven conformational changes at the catalytic sites and the central (DF) and peripheral stalks (EG1–3) (30). We propose that an allosteric structural change at the open catalytic site that is driven by release of inhibitory MgADP from the closed catalytic site in autoinhibited, WT V_1 by a yet unknown mechanism leads to the detachment of H_{CT} from its inhibitory position so that it can bind a_{NT} on V_o.

From studies in yeast it was shown that although C is required for binding of V_1 to V_o on yeast vacuolar membranes (36), deletion of H allows assembly of a labile but inactive complex (39). The requirement of C for association of V_1 with V_o is supported by our *in vitro* BLI experiments, wherein none of the V_1 mutants reconstituted with V_o in absence of C (Fig. S3). However, unlike *in vivo*, the presence of C along with $V_1\Delta H$, WT V_1, or V_1H_{wt} is not sufficient for reconstituting V_1V_o *in vitro*. This discrepancy is not due to a reduced affinity of C for

V_1, because we obtained a K_d of ~0.7 nM for the interaction between C and $V_1\Delta C$ (Fig. S4). A high-affinity interaction between C and $V_1\Delta C$ is consistent with substoichiometric amounts of C remaining associated with purified $V_1\Delta H$ and V_1 (16), as well as the reported K_d of ~42 nM for the EG–C interaction (31). However, tight and stable binding of C to $V_1\Delta C$ would be inconsistent with the observed release of C into the cytosol upon disassembly of V_1 from V_o (14), but, as shown here, ATP hydrolysis by V_1 leads to the rapid release of the V_1–C interaction, which likely explains why catalytically inactive enzyme does not disassemble upon glucose withdrawal (14). Although it has been reported that in the presence of the microtubule depolymerizing drug benomyl, C does not dissociate from V_1V_o upon glucose removal (40), it is possible that C under these conditions quickly rebinds EG3 once V_1 is in the autoinhibited state. In addition, a direct interaction between C and tubulin has been observed (40, 41), suggesting the possibility that, upon disassembly, C is sequestered by microtubules, preventing its reassociation with V_1 and/or V_o.

Although reincorporation of C upon glucose addition does not require the microtubule network (40), efficient (re)assembly of holo V-ATPase requires a heterotrimeric chaperone complex referred to as RAVE (regulator of H^+-ATPase of vacuolar and endosomal membranes). It has been proposed that upon receiving the signal for reassembly, RAVE recruits C and V_1 to V_o on vacuolar membranes by directly interacting with C, EG (as part of V_1), and a_{NT} (as part of V_o) (42). Under the *in vitro* conditions employed here, it takes ~2 h for a 1:1:2 mixture of V_1H_{chim}, V_oND, and C to complete reconstitution of $V_1H_{chim}V_oND$, a relatively slow process compared with the kinetics of reassembly observed *in vivo* (~5 min) (43). It is possible that the RAVE complex, by increasing the proximity of V_1, C, and V_o, facilitates the otherwise low-affinity interactions at the V_1–V_o interface (32), thereby accelerating reassembly.

From the here presented data, we conclude that the detachment of H_{CT} from V_1 and the presence of C subunit are required for the reassembly of V_1 with V_o (Fig. 5, *A–C*). In our *in vitro* reconstitutions, the association between V_1H_{chim} and V_oND is driven by the H_{CT}–a_{NT} interaction (Fig. 5*B*), but *in vivo*, the chain of events that leads to reassembly of autoinhibited V_1 and V_o are probably different, because H_{CT} is in its inhibitory conformation on V_1 (Fig. 5*A*). We propose that in yeast, upon receiving cellular signals, autoinhibited V_1 and C are first recruited to V_o (Fig. 5*D*), a process that is likely the rate-limiting step for reassembly. Our reason for this hypothesis is that even with the requirements for reassembly being met in our *in vitro* reconstitution of V_1H_{chim} and C with V_o, the rate of reassembly was slow. *In vivo*, recruitment of V_1 and C to V_o is facilitated and probably accelerated by the RAVE complex (42), but efficient (re)assembly *in vivo* requires additional factors such as the glycolytic enzymes aldolase (44) and phosphofructokinase (43), whose function in the process is currently not known. Once V_1 and C are recruited to V_o at the vacuolar membrane, inhibitory MgADP is released upon opening of the closed catalytic site by a yet unknown mechanism (Fig. 5*E*). The release of inhibitory MgADP allows MgATP hydrolysis to resume, with concomitant conformational changes at the catalytic sites and rotation of the central stalk (DF), structural changes that result in detachment of H_{CT} from V_1 (30) (Fig. 5*F*). The proximity of a_{NT} to V_1-detached H_{CT} facilitates the H_{CT}–a_{NT} interaction, a requirement for coupling of V_1 to V_o in the holo-enzyme (24). The H_{CT}–a_{NT} interaction stabilizes the peripheral conformation of a_{NT} such that the C_{foot}–EG2–a_{NT} ternary complex can be formed, thus completing functional (re)assembly (Fig. 5*C*).

V-ATPase regulation by reversible disassembly, originally discovered in lower eukaryotes, has been confirmed to be conserved in higher animals, including humans (19–21). Reconstitution of V_1 with V_o has been investigated for mammalian V-ATPase from bovine brain clathrin-coated vesicles and in one study, chaotropically removed V_1 reassembled with V_o on coated vesicle membranes upon dialysis, thereby regenerating ~80% of the initial MgATPase activity (45). In another study, *in vitro* reconstitution of coated vesicle V-ATPase from V_1 and V_o was shown to require the mammalian H subunit homolog SFD (sub-fifty-eight dimer) (46). However, in both cases, resulting V-ATPase complexes were not further characterized for subunit composition and structural integrity. Curiously, unlike yeast V_1, removal of SFD from bovine coated vesicle V_1 did not create a MgATP hydrolyzing V_1-ATPase, suggesting the presence of other regulatory mechanisms in mammalian V_1 (46). One of the likely reasons that few biochemical studies have focused upon the molecular mechanism of reversible disassembly in higher organisms is because mammalian V-ATPase is extraordinarily heterogeneous, with most subunits expressed as multiple isoforms or splice variants (including subunits H and *a*) (47), and to our knowledge, no *in vitro* system comparable to the one described here for the yeast V-ATPase has been reported for the mammalian enzyme. Yeast contains only one subunit with multiple isoforms (subunit *a*), and the two V-ATPase populations resulting from this single subunit difference appear to have different propensities to undergo dissociation, and only one of them requires the RAVE complex for (re)assembly (48, 49). It is likely that different isoform-containing enzymes in mammalian systems are subjected to differential regulatory mechanisms, resulting in variable propensities to dissociate. Because the human H_{CT} does not silence yeast V_1 but does facilitate efficient functional coupling in V_1V_o, it will be of interest to explore the mechanism of regulation by reversible disassembly as a function of subunit isoform composition of the mammalian system in greater detail by using the tools developed and presented here for the yeast enzyme.

Experimental procedures

Strains

The yeast strain SF838–5Aα deleted for the vma2 gene (B subunit) vma2Δ::Nat was a kind gift from Dr. Patricia Kane, SUNY Upstate Medical University. A plasmid containing the FLAG tag with a KanMX6 marker, pFA6a-6xGly-FLAG-kanMX6 was a gift from Dr. Mark Hochstrasser (50) (Addgene plasmid no. 20751). The primers vph1CTFlagFWD (gct gtt gct agt gca agc tct tcc gct tca agc GGG GGA GGC GGG GGT GGAA) and vph1CTFlagREV (cct gga tgt gga ttt cga ttc taa cgt tac ccc aag gca aat gat ggt cac tgg GAA TTC GAG CTC GTT TAA AC) were used to amplify the FLAG tag and

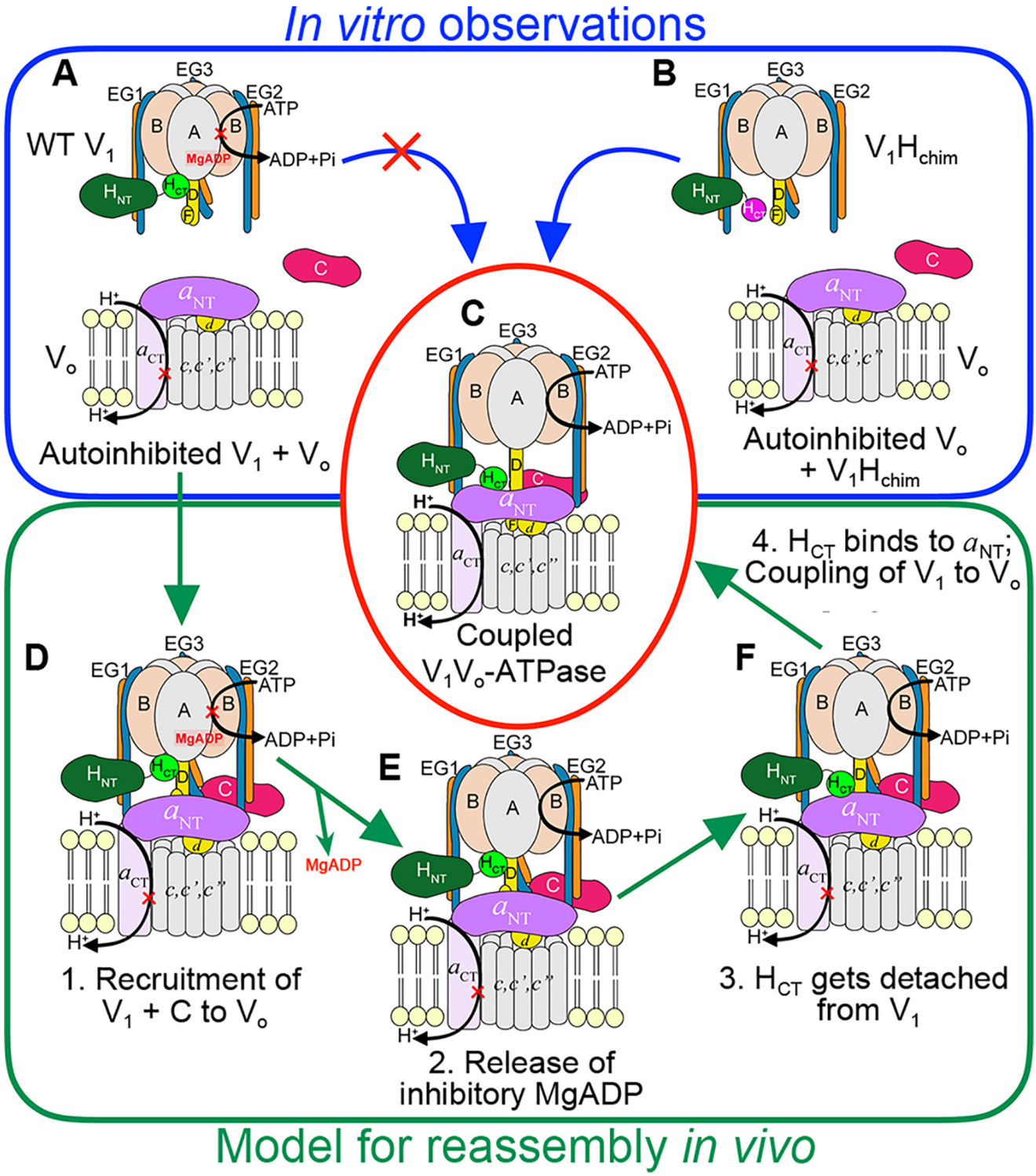

Figure 5. Model for reassembly of autoinhibited V_1 and V_o. *A–C*, our *in vitro* experiments have shown that although WT H containing V_1 does not readily bind V_oND (*A*), V_1H_{chim} spontaneously associates with V_oND (*B*) to form a structurally and functionally coupled V-ATPase, albeit at a slow rate. *C*, *in vivo*, however, V_1 exists in the autoinhibited conformation (*A*), and the rate of assembly with V_o is significantly faster (within 5 min). *D–F*, for *in vivo* (re)assembly, we propose that the following steps occur: step 1, recruitment of V_1 and subunit C to the vacuolar membrane (*D*); step 2, release of inhibitory MgADP (*E*); step 3, detachment of H_{CT} from its inhibitory position on V_1; and step 4, H_{CT} binding to a_{NT} (*F*). For further details, see text.

KanMX marker from pFA6a-6xGly-FLAG-kanMX6. The ~1.8-kb product was gel purified and used for homologous recombination to insert the FLAG-KanMX cassette in the C terminus of vph1 in the yeast strain SF838–5Aα vma2Δ::Nat using the same primers as above. Colonies were selected for growth on YPD G418 plates, and the insertion of the FLAG tag at the C terminus of vph1 was confirmed by sequencing. The construction of chimeric H subunit (H_{chim}) encoding the N-terminal domain from *Saccharomyces cerevisiae* (residues 1–352) and the C-terminal domain (349–483) of the human H

subunit into the yeast pRS316 vector has been discussed in Ref. 16. From the pRS316 vector, using the primers MalChimF (TTA GCC GGT ACC GGG AGC AAC GAA GAT ATT AAT GGA C) and MalChimR (TTA CCA AAG CTT TTA GCT TCG GGC GGC AG), H_{chim} was amplified. The primers additionally introduced the restriction sites 5′ KpnI and 3′ HindIII, which were used to insert the amplicon into a pMal vector. The resultant vector encoded MBP-tagged H_{chim} separated by a PreScission protease cleavage site, as confirmed by sequencing.

Purification of V_o and its reconstitution into endogenous vacuolar lipid

V_o was purified from yeast vacuoles and reconstituted into endogenous vacuolar lipid containing nanodiscs as described for V_1V_oND in Ref. 29. The steps are briefly described as follows.

Purification of biotinylated MSP

Biotinylated MSP was purified as described in Ref. 29. Briefly, BL21 (DE3) cells were co-transformed with the plasmids pHBPMSP1E3D1 and pBirAcm (encoding the BirA gene). The cells were grown in rich broth supplemented with 0.1 mM D-biotin, 34 μg/ml chloramphenicol, and 30 μg/ml kanamycin to an A_{595} of ~0.5 at 37 °C followed by induction using 0.5 mM isopropyl β-D-thiogalactopyranoside for 3–4 h. Harvested cells were purified as described in Ref. 26. Briefly, the cells were lysed by sonicating three times for 30 s. The lysate was cleared by centrifugation at 13,000 × *g* and passed over a nickel–nitrilotriacetic acid affinity column. The column was washed with 10 column volumes of the each of the three buffers: 40 mM Tris-HCl, 300 mM NaCl, and 1% Triton X-100, pH 8; 40 mM Tris-HCl, 300 mM NaCl, 50 mM sodium cholate, and 5 mM immidazole, pH 8; and 40 mM Tris-HCl, 300 mM NaCl, and 10 mM immidazole, pH 8. MSP was eluted with a 10–column volume gradient of the elution buffer (40 mM Tris-HCl, 300 mM NaCl, and 100 mM immidazole, pH 8). Purified biotinylated MSP was dialyzed into 25 mM Tris, 150 mM NaCl, 0.5 mM EDTA, pH 7.2; concentrated to ~5 mg/ml; snap frozen in liquid nitrogen; and stored at −80 °C until use.

Isolation of yeast vacuoles

Yeast vacuoles were isolated by flotation on a Ficoll density gradient as described in Ref. 51. Briefly, SF838–5Aα vma2Δ::Nat with a Flag tag on the C terminus of vph1 (*a* subunit) was grown to an A_{595} of ~1.0 in YPD pH 5. 12 liters of cells were harvested by centrifugation at 5000 × *g* for 30 min. The pellet was washed and resuspended in 100 ml of 1.2 M sorbitol with ~15 mg of zymolyase to form spheroplasts. The spheroplasts were recovered in 100 ml each of 2.4 M sorbitol and 2× YPD and then resuspended in buffer containing 12% Ficoll 400. The suspension was homogenized in a Dounce homogenizer and centrifuged at 71,000 × *g* for 40 min. Vacuole wafers from the top of the gradient were extracted, homogenized in buffer containing 8% Ficoll, and centrifuged at 71,000 × *g* for 40 min. The final vacuole wafers were resuspended in 1.5 mM Mes-Tris, pH 7.0, 5% glycerol, and 1 mM β-mercaptoethanol. Vacuolar protein concentration was measured using a modified BCA assay (18), and the vacuoles were frozen in liquid nitrogen until further use.

Extraction of V_o and reconstitution into lipid nanodiscs

Three batches of purified vacuoles (12 liters each) were typically used for one extraction as described in Ref. 29. Briefly, thawed vacuoles were combined, supplemented with protease inhibitors, and solubilized using 1.2 mg of *n*-dodecyl β-D-maltopyranoside/1 mg of vacuolar protein. To the detergent-solubilized sample, purified biotinylated MSP was added in a molar ratio of 1:50 (vacuolar protein:MSP). The mixture containing vacuolar protein, vacuolar lipids, and MSP was incubated at 4 °C for 1 h followed by detergent removal using biobeads. Reconstituted vacuolar membrane proteins in biotinylated and endogenous vacuolar lipid containing nanodiscs were subjected to anti-FLAG affinity chromatography to purify V_o-containing nanodiscs. The eluate from the FLAG column was then subjected to size-exclusion chromatography using a Superdex 200 1 × 30-cm column. Peak fractions from gel filtration were combined and concentrated using a Vivaspin 100,000 molecular weight cutoff concentrator.

Purification of the chimeric H subunit (H_{chim})

Escherichia coli Rosetta2 (Novagen) cells expressing N-terminal MBP-tagged H_{chim} were grown to an A_{600} of ~0.5 (in LB, 0.2% glucose, 50 μg/ml carbenicillin, and 34 μg/ml chloramphenicol), and expression was induced with 0.5 mM isopropyl β-D-thiogalactopyranoside at 30 °C for 4 h. Protein was purified using amylose affinity chromatography, and the MBP tag was cleaved with PreScission protease as previously described (31). The pH of the cleavage product was adjusted to 7 by overnight dialysis in 25 mM sodium phosphate, pH 7, 0.5 mM EDTA, and 5 mM β-mercaptoethanol. At pH 7, H_{chim} has a predicted charge of +3.5, whereas the predicted charge of MBP is −9 (Protein Calculator v3.4), allowing separation of the two proteins using cation exchange (carboxymethyl) chromatography. The cleaved MBP came off the carboxymethyl column in the flow through and wash steps, whereas pure H_{chim} was eluted in dialysis buffer supplemented with 100 mM NaCl. The preparation was subjected to a final step using a Superdex 200 1.6 × 50-cm size-exclusion chromatography column.

Purification of V_1 mutants and subunit C

WT V_1, $V_1\Delta H$ and $V_1\Delta C$ were purified from vma10Δ::KanMX (29), vma13Δ::KanMX, vma10Δ::Nat (34), and vma5Δ::Nat, vma10Δ::URA3 (16), respectively, as described in Ref. 16. In all cases, yeast strains were transformed with a pRS315 vector containing N-terminally FLAG tagged vma10 (G subunit) for affinity purification on αFLAG agarose (33). Cells were grown to an A_{595} of ~4 in synthetic dropout medium without leucine (SD −Leu) and harvested by centrifugation at 4000 × *g* for 15 min. The cells were lysed by ~15 passes through a microfluidizer (Microfluidics M-110L). Unbroken cells were pelleted by centrifugation at 4000 × *g* for 30 min, and the resultant supernatant was cleared by centrifugation at 13,000 × *g* for 40 min. Cleared lysate was subjected to affinity chromatography using αFLAG resin. The eluate from the αFLAG column

was concentrated and subjected to size-exclusion chromatography using a Superdex 200 1.6 × 50 cm column.

For preparation of V_1H_{chim} and V_1H_{wt}, $V_1\Delta H$ eluted from the αFLAG column was incubated for 1 h at 4 °C with a ~5-fold molar excess of either H_{chim} or H_{wt} (purified as in Ref. 30) to form the V_1H_{chim} and V_1H_{wt} complexes, respectively. V_1 bound to H_{chim} or H_{wt} was then separated from the excess of H_{chim} or H_{wt} by size-exclusion chromatography using a Superdex 200 1.6 × 50-cm column. Subunit C was purified as previously described (31).

Biolayer interferometry

Interaction of V_o with the purified V_1 mutants was screened using BLI, a light interference–based technique, similar to surface plasmon resonance. An Octet-RED system with streptavidin coated biosensors (Forte´Bio, SA biosensors, catalog no. 18-5019) were used for the experiments. All BLI experiments were conducted using 25 mM Tris-HCl, pH 7.2, 150 mM NaCl, 0.5 mM EDTA, 1 mM β-mercaptoethanol, 0.5 mg/ml BSA, except for experiments analyzing V_1H_{chim} release from immobilized MBP-C, which required 10 mg/ml BSA because of an increased propensity of chimeric H containing V_1 to bind nonspecificically to the BLI sensors. The temperature was maintained at 22 °C, with each biosensor stirred in 0.2 ml of sample at 1000 rpm and a standard measurement rate of 5 s^{-1}. Streptavidin-coated biosensors were prewetted in BLI buffer and then dipped in wells containing 3 μg/ml of biotinylated V_oND. A buffer control was included to show that none of the buffer components interacted with the sensors. Details of individual experiments have been described in the respective figure legends. The affinity of interaction between $V_1\Delta C$ and MBP-C was measured using anti-mouse IgG Fc capturing biosensors (FortéBio, AMC biosensors catalog no. 18-5088) as described (30).

ATPase activity assay

MgATPase activity of purified V_1 mutants and reconstitution mixtures (V_1 mutants + V_oND + subunit C) was measured using a coupled enzyme assay as described in Ref. 16. Briefly, 10 μg of the V_1 mutant was added to an assay mixture containing 1 mM $MgCl_2$, 5 mM ATP, 30 units/ml each of lactate dehydrogenase and pyruvate kinase, 0.5 mM NADH, 2 mM phosphoenolpyruvate, and 50 mM HEPES, pH 7.5, at 37 °C. The decrease of absorbance at 340 nm corresponding to the decline of NADH in the system was measured in the kinetics mode on a Varian Cary Bio100 spectrophotometer. In case of reconstitution mixtures, 20 μg of V_1 mutant with equimolar amounts of V_oND, and a 2× molar excess of C subunit was added to an assay containing 4 mM $MgCl_2$.

Author contributions—S. S., R. A. O., and S. W. conceptualization; S. S., R. A. O., and M. M. K. investigation; S. S. writing-original draft; R. A. O. and S. W. writing-review and editing; S. W. funding acquisition.

Acknowledgments—We thank Dr. Patricia Kane for reagents and many helpful discussions and Dr. Thomas Duncan for assistance with BLI data collection and analysis.

References

1. Forgac, M. (2007) Vacuolar ATPases: rotary proton pumps in physiology and pathophysiology. *Nat. Rev. Mol. Cell Biol.* **8,** 917–929 CrossRef Medline
2. Karet, F. E., Finberg, K. E., Nelson, R. D., Nayir, A., Mocan, H., Sanjad, S. A., Rodriguez-Soriano, J., Santos, F., Cremers, C. W., Di Pietro, A., Hoffbrand, B. I., Winiarski, J., Bakkaloglu, A., Ozen, S., Dusunsel, R., *et al.* (1999) Mutations in the gene encoding B1 subunit of H^+-ATPase cause renal tubular acidosis with sensorineural deafness. *Nat. Genet.* **21,** 84–90 CrossRef Medline
3. Thudium, C. S., Jensen, V. K., Karsdal, M. A., and Henriksen, K. (2012) Disruption of the V-ATPase functionality as a way to uncouple bone formation and resorption: a novel target for treatment of osteoporosis. *Curr. Protein Pept. Sci.* **13,** 141–151 CrossRef Medline
4. Williamson, W. R., and Hiesinger, P. R. (2010) On the role of v-ATPase V_0a_1-dependent degradation in Alzheimer disease. *Commun. Integr. Biol.* **3,** 604–607 CrossRef Medline
5. Sun-Wada, G. H., Toyomura, T., Murata, Y., Yamamoto, A., Futai, M., and Wada, Y. (2006) The a3 isoform of V-ATPase regulates insulin secretion from pancreatic β-cells. *J. Cell Sci.* **119,** 4531–4540 CrossRef Medline
6. Brown, D., Smith, P. J., and Breton, S. (1997) Role of V-ATPase-rich cells in acidification of the male reproductive tract. *J. Exp. Biol.* **200,** 257–262 Medline
7. Sennoune, S. R., Bakunts, K., Martínez, G. M., Chua-Tuan, J. L., Kebir, Y., Attaya, M. N., and Martínez-Zaguilan, R. (2004) Vacuolar H^+-ATPase in human breast cancer cells with distinct metastatic potential: distribution and functional activity. *Am. J. Physiol. Cell Physiol.* **286,** C1443–C1452 CrossRef Medline
8. Fais, S., De Milito, A., You, H., and Qin, W. (2007) Targeting vacuolar H^+-ATPases as a new strategy against cancer. *Cancer Res.* **67,** 10627–10630 CrossRef Medline
9. Kane, P. M. (2012) Targeting reversible disassembly as a mechanism of controlling V-ATPase activity. *Curr. Protein Pept. Sci.* **13,** 117–123 CrossRef Medline
10. Oot, R. A., Couoh-Cardel, S., Sharma, S., Stam, N. J., and Wilkens, S. (2017) Breaking up and making up: the secret life of the vacuolar H^+-ATPase. *Protein Sci.* **26,** 896–909 CrossRef Medline
11. Muench, S. P., Trinick, J., and Harrison, M. A. (2011) Structural divergence of the rotary ATPases. *Q. Rev. Biophys.* **44,** 311–356 CrossRef Medline
12. Kane, P. M. (1995) Disassembly and reassembly of the yeast vacuolar H^+-ATPase *in vivo*. *J. Biol. Chem.* **270,** 17025–17032 Medline
13. Sumner, J. P., Dow, J. A., Earley, F. G., Klein, U., Jäger, D., and Wieczorek, H. (1995) Regulation of plasma membrane V-ATPase activity by dissociation of peripheral subunits. *J. Biol. Chem.* **270,** 5649–5653 CrossRef Medline
14. Parra, K. J., and Kane, P. M. (1998) Reversible association between the V_1 and V_0 domains of yeast vacuolar H^+-ATPase is an unconventional glucose-induced effect. *Mol. Cell Biol.* **18,** 7064–7074 CrossRef Medline
15. Parra, K. J., Keenan, K. L., and Kane, P. M. (2000) The H subunit (Vma13p) of the yeast V-ATPase inhibits the ATPase activity of cytosolic V1 complexes. *J. Biol. Chem.* **275,** 21761–21767 CrossRef Medline
16. Oot, R. A., Kane, P. M., Berry, E. A., and Wilkens, S. (2016) Crystal structure of yeast V_1-ATPase in the autoinhibited state. *EMBO J.* **35,** 1694–1706 CrossRef Medline
17. Zhang, J., Myers, M., and Forgac, M. (1992) Characterization of the V_0 domain of the coated vesicle (H^+)-ATPase. *J. Biol. Chem.* **267,** 9773–9778 Medline
18. Couoh-Cardel, S., Milgrom, E., and Wilkens, S. (2015) Affinity purification and structural features of the yeast vacuolar ATPase V_o membrane sector. *J. Biol. Chem.* **290,** 27959–27971 CrossRef Medline
19. Trombetta, E. S., Ebersold, M., Garrett, W., Pypaert, M., and Mellman, I. (2003) Activation of lysosomal function during dendritic cell maturation. *Science* **299,** 1400–1403 CrossRef Medline
20. Stransky, L. A., and Forgac, M. (2015) Amino acid availability modulates vacuolar H^+-ATPase assembly. *J. Biol. Chem.* **290,** 27360–27369 CrossRef Medline

ASBMB

21. Bodzeta, A., Kahms, M., and Klingauf, J. (2017) The presynaptic v-ATPase reversibly disassembles and thereby modulates exocytosis but is not part of the fusion machinery. *Cell Rep.* **20,** 1348–1359 CrossRef Medline
22. Parra, K. J., Chan, C. Y., and Chen, J. (2014) *Saccharomyces cerevisiae* vacuolar H^+-ATPase regulation by disassembly and reassembly: one structure and multiple signals. *Eukaryot. Cell* **13,** 706–714 CrossRef Medline
23. Zhao, J., Benlekbir, S., and Rubinstein, J. L. (2015) Electron cryomicroscopy observation of rotational states in a eukaryotic V-ATPase. *Nature* **521,** 241–245 CrossRef Medline
24. Liu, M., Tarsio, M., Charsky, C. M., and Kane, P. M. (2005) Structural and functional separation of the N- and C-terminal domains of the yeast V-ATPase subunit H. *J. Biol. Chem.* **280,** 36978–36985 CrossRef Medline
25. Mazhab-Jafari, M. T., Rohou, A., Schmidt, C., Bueler, S. A., Benlekbir, S., Robinson, C. V., and Rubinstein, J. L. (2016) Atomic model for the membrane-embedded V_O motor of a eukaryotic V-ATPase. *Nature* **539,** 118–122 CrossRef Medline
26. Stam, N. J., and Wilkens, S. (2017) Structure of the lipid nanodisc-reconstituted vacuolar ATPase proton channel: definition of the interaction of rotor and stator and implications for enzyme regulation by reversible dissociation. *J. Biol. Chem.* **292,** 1749–1761 CrossRef Medline
27. Roh, S. H., Stam, N. J., Hryc, C. F., Couoh-Cardel, S., Pintilie, G., Chiu, W., and Wilkens, S. (2018) The 3.5-A cryoEM structure of nanodisc-reconstituted yeast vacuolar ATPase V_o proton channel. *Mol. Cell* **69,** 993–1004.e3 CrossRef Medline
28. Parra, K. J., and Kane, P. M. (1996) Wild-type and mutant vacuolar membranes support pH-dependent reassembly of the yeast vacuolar H^+-ATPase *in vitro*. *J. Biol. Chem.* **271,** 19592–19598 CrossRef Medline
29. Sharma, S., and Wilkens, S. (2017) Biolayer interferometry of lipid nanodisc-reconstituted yeast vacuolar H^+-ATPase. *Protein Sci.* **26,** 1070–1079 CrossRef Medline
30. Sharma, S., Oot, R. A., and Wilkens, S. (2018) MgATP hydrolysis destabilizes the interaction between subunit H and yeast V1-ATPase, highlighting H's role in V-ATPase regulation by reversible disassembly. *J. Biol. Chem.* **293,** 10718–10730 CrossRef Medline
31. Oot, R. A., and Wilkens, S. (2010) Domain characterization and interaction of the yeast vacuolar ATPase subunit C with the peripheral stator stalk subunits E and G. *J. Biol. Chem.* **285,** 24654–24664 CrossRef Medline
32. Oot, R. A., and Wilkens, S. (2012) Subunit interactions at the V_1–V_o interface in yeast vacuolar ATPase. *J. Biol. Chem.* **287,** 13396–13406 CrossRef Medline
33. Zhang, Z., Charsky, C., Kane, P. M., and Wilkens, S. (2003) Yeast V1-ATPase: affinity purification and structural features by electron microscopy. *J. Biol. Chem.* **278,** 47299–47306 CrossRef Medline
34. Diab, H., Ohira, M., Liu, M., Cobb, E., and Kane, P. M. (2009) Subunit interactions and requirements for inhibition of the yeast V_1-ATPase. *J. Biol. Chem.* **284,** 13316–13325 CrossRef Medline
35. Oot, R. A., Huang, L. S., Berry, E. A., and Wilkens, S. (2012) Crystal structure of the yeast vacuolar ATPase heterotrimeric EGC(head) peripheral stalk complex. *Structure* **20,** 1881–1892 CrossRef Medline
36. Curtis, K. K., Francis, S. A., Oluwatosin, Y., and Kane, P. M. (2002) Mutational analysis of the subunit C (Vma5p) of the yeast vacuolar H^+-ATPase. *J. Biol. Chem.* **277,** 8979–8988 CrossRef Medline
37. Wilkens, S., Vasilyeva, E., and Forgac, M. (1999) Structure of the vacuolar ATPase by electron microscopy. *J. Biol. Chem.* **274,** 31804–31810 CrossRef Medline
38. Zhang, Z., Zheng, Y., Mazon, H., Milgrom, E., Kitagawa, N., Kish-Trier, E., Heck, A. J., Kane, P. M., and Wilkens, S. (2008) Structure of the yeast vacuolar ATPase. *J. Biol. Chem.* **283,** 35983–35995 CrossRef Medline
39. Ho, M. N., Hirata, R., Umemoto, N., Ohya, Y., Takatsuki, A., Stevens, T. H., and Anraku, Y. (1993) VMA13 encodes a 54-kDa vacuolar H^+-ATPase subunit required for activity but not assembly of the enzyme complex in *Saccharomyces cerevisiae*. *J. Biol. Chem.* **268,** 18286–18292 Medline
40. Tabke, K., Albertmelcher, A., Vitavska, O., Huss, M., Schmitz, H. P., and Wieczorek, H. (2014) Reversible disassembly of the yeast V-ATPase revisited under *in vivo* conditions. *Biochem. J.* **462,** 185–197 CrossRef Medline
41. Xu, T., and Forgac, M. (2001) Microtubules are involved in glucose-dependent dissociation of the yeast vacuolar $[H^+]$-ATPase *in vivo*. *J. Biol. Chem.* **276,** 24855–24861 CrossRef Medline
42. Smardon, A. M., Nasab, N. D., Tarsio, M., Diakov, T. T., and Kane, P. M. (2015) Molecular interactions and cellular itinerary of the yeast RAVE (regulator of the H^+-ATPase of vacuolar and endosomal membranes) complex. *J. Biol. Chem.* **290,** 27511–27523 CrossRef Medline
43. Chan, C. Y., and Parra, K. J. (2014) Yeast phosphofructokinase-1 subunit Pfk2p is necessary for pH homeostasis and glucose-dependent vacuolar ATPase reassembly. *J. Biol. Chem.* **289,** 19448–19457 CrossRef Medline
44. Lu, M., Ammar, D., Ives, H., Albrecht, F., and Gluck, S. L. (2007) Physical interaction between aldolase and vacuolar H^+-ATPase is essential for the assembly and activity of the proton pump. *J. Biol. Chem.* **282,** 24495–24503 CrossRef Medline
45. Puopolo, K., and Forgac, M. (1990) Functional reassembly of the coated vesicle proton pump. *J. Biol. Chem.* **265,** 14836–14841 Medline
46. Xie, X. S., Crider, B. P., Ma, Y. M., and Stone, D. K. (1994) Role of a 50–57-kDa polypeptide heterodimer in the function of the clathrin-coated vesicle proton pump. *J. Biol. Chem.* **269,** 25809–25815 Medline
47. Toei, M., Saum, R., and Forgac, M. (2010) Regulation and isoform function of the V-ATPases. *Biochemistry* **49,** 4715–4723 CrossRef Medline
48. Kawasaki-Nishi, S., Nishi, T., and Forgac, M. (2001) Yeast V-ATPase complexes containing different isoforms of the 100-kDa a-subunit differ in coupling efficiency and *in vivo* dissociation. *J. Biol. Chem.* **276,** 17941–17948 CrossRef Medline
49. Smardon, A. M., Diab, H. I., Tarsio, M., Diakov, T. T., Nasab, N. D., West, R. W., and Kane, P. M. (2014) The RAVE complex is an isoform-specific V-ATPase assembly factor in yeast. *Mol. Biol. Cell* **25,** 356–367 CrossRef Medline
50. Funakoshi, M., and Hochstrasser, M. (2009) Small epitope-linker modules for PCR-based C-terminal tagging in *Saccharomyces cerevisiae*. *Yeast* **26,** 185–192 CrossRef Medline
51. Uchida, E., Ohsumi, Y., and Anraku, Y. (1985) Purification and properties of H^+-translocating, Mg^{2+}-adenosine triphosphatase from vacuolar membranes of *Saccharomyces cerevisiae*. *J. Biol. Chem.* **260,** 1090–1095 Medline